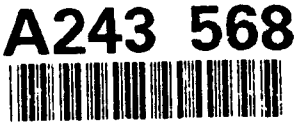

SM Report 88-8

DYNAMIC MEASUREMENT OF THE J INTEGRAL IN DUCTILE METALS: COMPARISON OF EXPERIMENTAL AND NUMERICAL TECHNIQUES

by

ALAN T. ZEHNDER*
ARES J. ROSAKIS
SRIDHAR KRISHNASWAMY

August 1988

GRADUATE AERONAUTICAL LABORATORIES
CALIFORNIA INSTITUTE OF TECHNOLOGY
PASADENA, CALIFORNIA 91125

* currently at the Department of Theoretical and Applied Mechanics, Cornell University, Ithaca, New York 14853-1503

ABSTRACT

Experiments and analyses designed to develop an extension of the method of caustics to applications in dynamic, elastic-plastic fracture mechanics are described. A relation between the caustic diameter, D, and the value of the J integral was obtained experimentally and numerically for a particular statically loaded specimen geometry (three point bend) and material (4340 steel). Specimens of the same geometry and material were then loaded dynamically in impact. The resulting caustics, recorded using high speed photography, were analyzed on the basis of the J versus D relation to determine the time history of the dynamic value of J, $J^d(t)$. The history of J^d thus obtained is compared with good agreement to an independent determination of $J^d(t)$ based on a two dimensional, dynamic, elastic-plastic finite element analysis, which used the experimentally measured loads as traction boundary conditions.

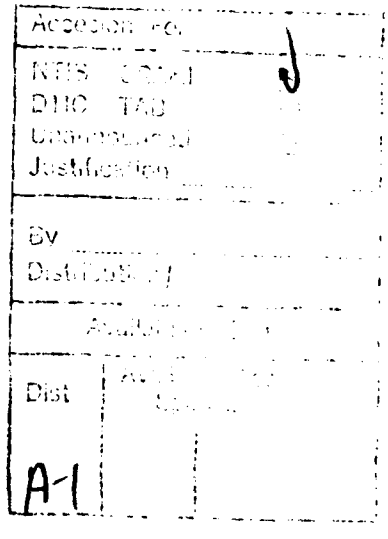

1. INTRODUCTION

For two-dimensional, monotonically loaded, stationary cracks, the J integral, defined by Rice[1], is a path independent line integral evaluated over an open contour surrounding the crack tip, and its value is a measure of the intensity of the crack tip strain singularity[2,3]. The critical value of J for crack initiation is commonly used as a measure of fracture toughness in ductile materials.

For three-dimensional plates of uniform thickness containing through cracks, the J integral is defined over a cylindrical surface surrounding the *entire* crack front (see Budiansky and Rice[4] and Broberg[5]). For monotonic loading or for materials obeying the deformation theory of plasticity, the value of this integral is independent of the choice of surface. In addition, for materials obeying the deformation theory of plasticity this integral may be interpreted as the energy release rate for self-similar crack extension along the entire crack front. A per thickness value, denoted in the rest of this paper as J, can be obtained by dividing the above surface integral by the thickness of the plate. This value can be shown to be equal to the through the thickness average of the *local* definition of J [6,7,8] (denoted here by $\hat{J}(x_3)$, where x_3 is the coordinate through the thickness of the body). Assuming that the variation of the intensity of the crack tip strain singularity through the thickness of the body is locally governed by $\hat{J}(x_3)$, the value J may be interpreted as an average of the intensity of the fields through the thickness.

Since the experimental evaluation of the local value, $\hat{J}(x_3)$, along the crack front is not possible, the goal of experiments involving plates of uniform thickness can only be to measure the average value of J corresponding to crack initiation. The availability of analytical models relating J and $\hat{J}$ for specific specimen geometries *may* subsequently make it possible to investigate the validity of a local criterion for crack initiation at the center plane of the specimen.

For dynamically loaded cracks, J loses its surface independence. However, if J is defined only in the limit as the cylindrical surface shrinks to the crack front, then for materials obeying the deformation theory of plasticity, this limiting value of J equals the energy release rate. For materials obeying incremental plasticity, this value is not equal to the energy release rate but may still have the interpretation of the average intensity of the

crack tip strain singularity through the thickness. Assuming that this is true, it is expected that dynamic fracture toughness may still be characterized by the J integral, keeping in mind that now this integral is evaluated over a cylindrical surface which has shrunk to the crack front. Although there are well proven experimental techniques for measruing J under static loading, few proven experimental techniques exist for measurement of the time history of J, $J^d(t)$, under dynamic loading conditions.

For example in quasi-static experiments J may be accurately inferred from established procedures based on the measurement of boundary conditions. However, such procedures generally fail to accurately determine J under dynamic loading. Nevertheless there exist cases where careful choice of specimen geometry and loading histories allows for the measurement of J^d based on the use of dynamic boundary value measurements interpreted on the basis of quasi-static formulas for J. A characteristic example of such an approach is described by Costin, Duffy and Freund[9], who estimate J^d by measuring the transient load displacement records and by using the *quasi-static* formula for deeply notched round bars. A dynamic finite element analysis of their particular specimen geometry and material, described by Nakamura, Shih and Freund[10], has indeed confirmed that this approximate procedure gives accurate values of J^d, at least for times close to the time of crack initiation. Unfortunately, such a conclusion will not hold for other specimen geometries [11,12] where alternative methods of measuring $J^d(t)$ should be investigated. A recently developed procedure, reported by Douglas and Suh [13] and by Sharpe, Douglas and Shapiro [14], provides an alternative way of obtaining dynamic fracture toughness at high loading rates. In their work, the results of a rate sensitive dynamic finite element analysis modeling a three point bend specimen made of HY-100 steel, loaded by a projectile, are compared to experimental measurements performed by means of the interferometric strain-displacement gauge technique described in [14]. The goal of the comparison is to provide the critical value of CTOD (crack tip opening displacement) and thus the critical value of J, corresponding to crack initiation.

An additional factor that complicates dynamic fracture testing procedures in ductile solids is the question of the accurate determination of the fracture initiation time. For quasi-static experiments, crack initiation can be detected by a number of techniques, for

example those involving measurement of changes in the electrical resistivity or variations of the compliance of the specimen. In dynamic testing, however, crack initiation may be very difficult to detect unless local optical crack tip measurements are possible.

Optical techniques have a number of advantages for dynamic, local crack tip measurements. Their interpretation does not rely on prior knowledge of the complex, transient boundary conditions or on the availability of complicated, dynamic analytical or numerical models of the experiments. Their time response is virtually instantaneous compared to the time scale of the mechanical response. Finally, due to the local nature of the measurements, optical methods can be expected to be sensitive enough to detect local events such as the onset of crack tunneling or gross crack initiation. In this work we describe the initial states for development of such an optical technique.

The optical method chosen is the method of caustics by reflection, which has already found many useful applications in elastic, dynamic fracture mechanics. This paper describes experiments designed to develop an extension of the method of caustics to applications in dynamic *elastic-plastic* fracture mechanics.

The method of caustics was originally developed by Manogg [15] for measuring the stress intensity factor in thin, transparent, elastic plates. A series of important contributions on the subject is also summarized by Theocaris [16]. The first extensions of the method of caustics to elastic-plastic fracture were made by Rosakis and Freund [17] and Rosakis, Ma, and Freund [18], based on the assumption of validity of the plane stress, HRR, asymptotic crack tip field [2,3] and it was demonstrated that under certain conditions the value of the J integral *can* be measured with caustics. Nonetheless, the recent work of Zehnder, Rosakis and Narasimhan [19] showed that the two-dimensional asymptotic approach severely limits the applicability of the method. This is true because such an analysis cannot deal with either three-dimensional effects near the crack tip or with large scale yielding effects, both characteristic of finite test specimens.

A new approach is taken here that allows for accurate measurement of the thickness average of J for any planar test specimen geometry and material [20]. In brief, the approach is to make a calibration of J versus the caustic diameter, D, for a particular specimen geometry (three point bend specimen) and material. It is shown that this calibration may

be performed experimentally or numerically with equal accuracy.

The relation between D and J is then used for the interpretation of caustics obtained in dynamic experiments. The dynamic experiments use the same three point bend specimen geometry as in the static tests, but loaded in a drop weight tower. The resulting caustic patterns are recorded with a rotating mirror high-speed camera and provide a time history of J^d up to the point of crack initiation. Crack initiation times are obtained by observations of changes in caustic shapes corresponding to the tunneling action through the specimen.

This measurement is to our knowledge the first direct optical measurement of $J^d(t)$ performed under dynamic loading conditions. Comparison is made between the $J^d(t)$ record measured by caustics and $J^d(t)$ obtained by a dynamic finite element calculation modeling the impact event.

The success of this approach suggests that the procedure discussed below can be used as a method for measuring $J^d(t)$ in any plate specimen geometry regardless of loading rate.

2. CAUSTICS BY REFLECTION

2.1 The mapping equations

Consider the flat surface of an opaque plate specimen of uniform thickness h, containing a through crack. In the undeformed state, this surface, assumed to be perfectly reflective, will occupy a region in the x_1, x_2 plane at $x_3 = 0$. When loads are applied on the lateral boundaries of the plate, the resulting change in thickness of the plate specimen is nonuniform and the equation of the deformed specimen surface can in general be expressed as:

$$x_3 + f(x_1, x_2) = 0. \tag{2.1}$$

Consider further, a family of light rays parallel to the x_3-axis, incident on the reflecting surface. Upon reflection, the light rays will deviate from parallelism (see Figure 1). If certain geometrical conditions are met by the reflecting surface, then the virtual extensions of the reflected rays (dashed lines) will form an envelope which is a three-dimensional surface in space. This surface, called the *"caustic surface"*, is the locus of points of highest density of rays (maximum luminosity) in the virtual image space. The virtual extensions of the rays are tangent to the caustic surface. The reflected light field is recorded on a camera positioned in front of the specimen. The focal plane of this camera, which will be called the *"screen"*, is located behind the plane $x_3 = 0$ (occupied by the reflector in the undeformed state) and intersects the caustic surface at the plane $x_3 = -z_0$, $z_0 \geq 0$. On the *"screen"*, a cross section of the caustic surface is observed as a bright curve (the *caustic curve*), bordering a dark region (the *shadow spot*). The resulting optical pattern depends on the nature of the function $f(x_1, x_2)$ and on the focal distance z_0.

The reflection process can be viewed as a mapping of points (x_1, x_2) of the plane occupied by the reflector in the undeformed state, onto points (X_1, X_2) of the plane $x_3 = -z_0$ (the *"screen"*). The mapping equations based on geometrical optics are given by [21]:

$$\underline{X} = \underline{x} - 2(z_0 - f)\frac{\nabla f}{1 - |\nabla f|^2}$$

where $\underline{X} = X_\alpha \underline{e}_\alpha$, $\underline{x} = x_\alpha \underline{e}_\alpha$, and $\underline{e}_\alpha$ denote unit vectors. In the subsequent discussion Greek subscripts have the range 1,2.

When $z_0 \gg f$, as is usually the case in most practical applications, the above simplifies to

$$\underline{X} = \underline{x} - 2z_0 \nabla f. \tag{2.3}$$

Relations (2.3) are the mapping equations what will be used in the rest of this discussion.

2.2 The initial curve and its significance

Equation (2.2), or its approximation (2.3), is a mapping of the points on the reflecting surface onto points on the *"screen"*. If the *"screen"* intersects the caustic surface, then the resulting caustic curve on the *"screen"* is a locus of points for which the determinant of the Jacobian matrix of the mapping equations (2.3) must vanish or

$$I(x_1, x_2, z_0) = det[X_{\alpha,\beta}] = det[\delta_{\alpha,\beta} - 2z_0 f_{\alpha,\beta}] = 0. \tag{2.4}$$

The above is a necessary and sufficient condition for the existence of a caustic curve. The locus of points on the reference plane ($x_1, x_2, x_3 = 0$) for which the Jacobian vanishes is called the *initial curve* and its equation is given by (2.4). All points on the initial curve map onto the caustic curve. In addition, all points inside and outside this curve map *outside* the caustic. Since the light that forms the caustic curve originates from the *initial curve*, essential information conveyed by the caustic comes from that curve *only*.

Equation (2.4), defining the initial curve, depends parametrically on z_0. Thus by varying z_0, the initial curve position may be varied. If z_0 is large, then the initial curve will be located far from the crack tip. If z_0 is small, then the initial curve will be close to the crack tip. Variation of z_0 can easily be achieved experimentally by simply varying the focal plane of the recording camera system. This is an essential property of the method of caustics and it can be utilized to "scan" the near tip region and to obtain information regarding the nature of deformation field at different distances from the crack tip. For the case of a crack tip surrounded by a plastic zone, varying z_0 will move the *"initial curve"* inside or outside the plastic zone, providing information on the plastic strains as well as on the surrounding elastic field.

2.3 The interpretation of caustics on the basis of plane stress analyses

The discussion of the previous section is intentionally kept as general as possible, and is not restricted by the form of the function $f(x_1, x_2)$ that describes the shape of

the deformed specimen surface. In general, $f(x_1, x_2)$ can be identified as the out of plane displacement field $u_3(x_1, x_2)$ evaluated on the surface of the plate specimen.

For a cracked plate of uniform thickness and finite, in-plane dimensions, u_3 will depend on the constitutive law of the material, on the applied load, and on the details of the specimen geometry (in-plane dimensions and thickness). Given the lack of full-field, three-dimensional analytical solutions in fracture mechanics, such information must be obtained by numerical computation. Nevertheless, there exist certain special cases where available asymptotic solutions, based on two-dimensional analyses, may provide adequate approximations for the surface out of plane displacement field $u_3(x_1, x_2)$. In particular, it is often argued that conditions of plane stress will dominate in thin, cracked plates provided that both the crack length and the in-plane dimensions are large compared to the plate thickness. In such cases, $u_3(x_1, x_2)$ may be *approximated* by means of available analytical solutions based on plane stress analyses.

2.3.1 Caustics obtained on the basis of plane stress asymptotic crack tip fields in linear elastostatics.

In linear elastic fracture mechanics, the principal application of the method of caustics is to the direct measurement of the mode-I and mode-II stress intensity factors. By substitution of the u_3 displacements for a Mode-I, plane stress crack [22] into equations (2.3) and (2.4), it was shown by Manogg [15] (see also Theocaris [16] and Beinert and Kalthoff [23]) that K_I is related to the maximum transverse diameter D of the caustic (width of caustic in the direction perpendicular to the crack line) by

$$K_I = \frac{ED^{5/2}}{10.7 z_0 \nu h}, \tag{2.5}$$

where E is the elastic modulus, ν is the Poisson's ratio, h is the specimen thickness, and K_I is the mode-I stress intensity factor.

The equation for the initial curve is obtained directly from (2.4) and can be shown to be a circle of radius r_0 where

$$r_0 = 0.316D = \left(\frac{3h\nu K_I z_0}{2E\sqrt{2\pi}} \right)^{2/5} \tag{2.6}$$

It should be observed here that for a given K_I, $r_0 \sim z_0^{2/5}$. A variation in z_0, the distance behind the specimen at which the camera is focused, will result in changes in r_0.

2.3.2 Caustics obtained on the basis of the asymptotic, plane stress HRR field.

For stationary cracks and within the framework of small displacement gradients and proportional stress histories the value of the J-integral can be considered as a plastic strain intensity factor. The viewpoint is adopted here that J is the scalar amplitude of the deformed shape of the surface of an elastic-plastic fracture specimen at points within the region of dominance of the *plane stress* HRR field.

Substitution of the u_3 displacement given by the asymptotic plane stress HRR fields into equations (2.3) and (2.4) provides a relation between D and J, found by Rosakis, Ma, and Freund [18] to be

$$J = S_n \frac{\sigma_0^2}{E} \left(\frac{E}{\sigma_0 z_0 h} \right)^{\frac{n+1}{n}} D^{\frac{3n+2}{n}}, \tag{2.7}$$

where σ_0 is the yield stress, n is the hardening exponent for the Ramberg-Osgood material model and S_n is a scalar function of n tabulated in [18]. Unlike the elastic case, the initial curve is no longer circular; its shape depends on the hardening exponent n of the material.

It should be noted at this point that equations (2.5) and (2.7) are obtained under the assumption of the validity of particular *asymptotic plane stress* fields at the vicinity of the crack tip. It is also implicitly assumed that the *initial curves* generating the caustics lie within the regions of dominance of such fields.

3. THE TECHNIQUE FOR MEASURING J

3.1 General applicability of caustics in the absence of asymptotic plane stress dominance

The interpretation of caustics on the basis of plane stress, asymptotic fields, limits the applicability of the method to specific, restricted specimen geometries where such fields may adequately describe the near tip out of plane displacements. However, in many cases of practical interests, sizeable regions of three dimensionality surrounding the crack tip may preclude the existence of regions of dominance of two-dimensional (plane stress) asymptotic expressions for u_3. In such cases, caustics can still be accurately analyzed provided that $u_3(x_1, x_2)$ and thus $f(x_1, x_2)$ can be obtained by means of full field three-dimensional numerical calculations modeling the specific specimen geometry and material characteristics.

In this section, an approach is described which will allow for the prediction of the relation between the average value of J in cracked specimens of uniform thickness and the caustics diameter,D, regardless of specimen geometry, dimensions and load level. In brief this approach consists of a calibration of J versus the caustic diameter, D, for a particular three-dimensional specimen configuration and a particular value of z_0. This calibration is performed first experimentally and then numerically by means of a three-dimensional elastic-plastic finite element calculation simulating the specimen. The two calibrations are compared to establish agreement between the experiment and the numerical calibration. The resulting relation between J and D, fully reflects the complex three-dimensional and nonlinear nature of the near tip deformation fields.

As one might think, a specimen dependent calibration of this sort is not of particular use for *static* measurements of J where other techniques, based on boundary value measurements, can be used. On the other hand the availability of such a calibration may prove very useful for the optical measurements of the time history of the dynamic value of $J(J^d(t))$. In particular, if the same specimen geometry and material are subjected to dynamic loading (e.g., impact), the resulting caustic patterns, recorded by means of a high speed camera, may be analyzed on the basis of such a calibration.

It should be noted that since this procedure makes use of a "static" calibration relation

between J and D, it is expected to provide accurate results for J^d only if the material tested is relatively rate insensitive, (e.g., 4340 carbon steel at room temperature [24]). In this work, see section 4, the accuracy of the approach outlined above is examined for the case of a 4340 steel three point bend specimen loaded dynamically in a drop weight tower. The time history of J^d thus obtained is compared to an entirely independent prediction of J^d obtained on the basis of a fully dynamic elastoplastic finite element calculation, which made use of the experimentally measured boundary loads as traction boundary conditions.

3.2 The static experiments

The static experiments (discussed in detail in [25]) used three point bend specimens (numbers 67 and 69) with a 4:1 length to width ratio. The specimen dimensions are given in Figure 2. The material used was a 4340 carbon steel, heat treated at 843°C for 1.5 hours, oil quenched, then annealed for 1 hour at 538°C. The yield stress was $\sigma_0 = 1030\,MPa$, and the hardening experiment $n = 22.5$ for a fit to the piecewise power hardening law. In uniaxial tension this is equivalent to

$$\frac{\epsilon}{\epsilon_0} = \begin{cases} \frac{\sigma}{\sigma_0} & \sigma \leq \sigma_0 \\ \left(\frac{\sigma}{\sigma_0}\right)^n & \sigma > \sigma_0 \end{cases}, \tag{3.1}$$

where ϵ_0 is the yield strain.

The experiments proceeded by loading the specimen in small steps. During the loading, the load cell and the load-point displacement signals were recorded. When the loading was stopped at a particular step, caustics photographs were recorded. This process was repeated until the point of fracture initiation.

The load and load point displacement were recorded with a 100,000 lb. capacity load cell and a strain gage extensometer. The specimen geometry was chosen to take advantage of the load-displacement methods for estimating the J integral. For ductile three-point bend specimens, Rice, Paris, and Merkle[26] demonstrated that J may be estimated by integration of the load-displacement record as follows:

$$J = \frac{2}{hC} \int_0^{\delta_c} P d\delta_c \tag{3.2}$$

where P is the load applied to the specimen, h is the specimen thickness and C is the uncracked ligament length. The quantity δ_c is the load-point displacement due to the

presence of the crack, i.e., $\delta_c = \delta - \delta_{nc}$ where δ is the total load point displacement and δ_{nc} is the load-point displacement of an uncracked, elastic beam of the same dimensions as the fracture specimen.

The resulting J integral, plotted as a function of load P, is given in Figure 3. Shown in the figure are J calculated from equation (3.2) using the experimental results and J calculated from the numerical analysis (see next section). The agreement between the *numerical* and *experimental* results is quite good, indicating that J may be calculated accurately either way.

3.3 The static 3-D numerical calculation

The numerical calculation, described in detail by Narasimhan and Rosakis [27] modeled in three dimensions, one quarter of the three point bend specimen shown in Fig. 2, using five layers of elements for *half* the thickness. An incremental J_2 plasticity theory was used. The material obeyed the von Mises yield condition and followed the piecewise power hardening law of equation (3.1) with $n = 22.5$ and $\sigma_0 = 1030\,MPa$, corresponding to the material used in the experiment. The J integral calculated numerically is shown here as a function of load in Fig. 3. This J corresponds to an integral evaluated over a cylindrical surface surrounding the entire crack front and as discussed earlier, is equal to the thickness average of the *local* definition and J along the crack front, (see [8]).

3.4 The relation between J and D.

In earlier work reported in [25,27], the resolution and accuracy of the three-dimensional elastic-plastic calculation was established by comparison of the numerical results for the out of plane surface displacements u_3 to experimental measurements of u_3 obtained by means of Twyman-Green interferometry. The excellent agreement of the analysis and the experiments reported in [25] indicate that the numerical calculation has sufficient refinement to generate accurately numerical (synthetic) caustic patterns which can be used to provide the relation between J and D.

Caustics are first recorded experimentally for specimens 67 and 69 using a *fixed value* of $z_0 = 100\,cm$. The sequence of caustic patterns for increasing loads up to fracture initiation, is shown in Figure 4. For the same value of z_0, and the same loads, caustics are also generated numerically from the results of the 3-D finite element analysis. This

was achieved by smoothing the u_3 displacements at the specimen surface obtained by the numerical solution using a least squares numerical scheme as described by Narasimhan and Rosakis [28]. Caustic patterns were simulated by mapping rays point by point from this smoothed surface using equation (2.3). The numerically simulated caustics are also shown in Figure 4. All of the caustic curves, both experimental and numerical are reproduced here in the same scale. The values of J shown in the figure are related to the applied load through the $J - P$ record of Figure 3. Figure 4 shows that there is good agreement, in shape and in size, between the experimental and numerical caustics.

Both experimental and numerical results were used to obtain a relation between caustic diameter, D, and the J integral which is shown in Figure 5 in a nondimensional form. J was obtained from Figure 3 and D was measured directly from the experimentally and numerically generated caustics. Also shown in the figure are the J vs. D relations obtained on the basis of the *plane stress* elastic analysis, equation (2.5), and on the basis of the *plane stress* HRR field, equation (2.7). The solid line in Figure 5 is a fit through the experimental and numerical data points.

It is seen that the experimental and numerical results are in excellent agreement. This demonstrates that such an approach can provide an accurate analysis of caustics in the form of a calibration for measuring the J integral. The best curve fit shown in Figure 5 serves here as an empirical relationship between the caustic diameter and the J integral when the relationship based on two-dimensional asymptotic analyses are invalid. This relationship is valid only for the specimen geometry and material tested here and only for $z_0 = 100\,cm$. It should be noted here that the relation between J and D reported here, fully reflects the complex three-dimensional and nonlinear nature of the near-tip deformation fields and does not suffer from the shortcomings of relation (2.7), discussed in section 2.

It should also be emphasized once more that this calibration relation is strictly geometry, material and z_0 dependent and as such its usefulness is very restricted in a static experiment where alternative ways of evaluating J may be desirable. On the other hand, in a dynamic setting such a calibration can prove invaluable for the dynamic measurement of the time history of J, as described in the next section.

4. DYNAMIC FRACTURE EXPERIMENTS

The relationship between J and D discussed above will be applied here for the measurement of dynamic fracture toughness of a ductile metal (annealed 4340 steel).

4.1 Description of experiments

Three point bend specimens (numbered 70-77) of the same geometry, material and heat treatment as the specimens used for the static experiments (see Fig. 2) were used for the dynamic experiments. As was done for the statically loaded specimens, the initial crack length of $30\,mm$ was machined using a wire electric discharge machine (EDM) producing an initial crack tip diameter of $0.3\,mm$. Two specimens (numbered 74 and 75) were fatigue-cracked an additional $4.0\,mm$.

The test specimens were dynamically loaded in 3-point bending by the Dynatup 8100A drop weight tester shown in Fig. 6. The drop weight is variable from 1910 N to 4220 N (430 lb. - 950 lb.) and the maximum impact speed is $10\,m/s$. In the present experiments the weight was 1910 N and impact speeds of 5 and 10 m/s were used. The impact speeds and initial crack tip conditions are summarized in Table 1 along with estimates for critical values of J. The tup (impact hammer) and the supports are instrumented with semiconductor strain gages allowing for the recording of the dynamic loads on a Nicolet 4094 digital oscilloscope.

Two LED-Photodiode switches mounted on the drop weight tower provide trigger signals for the camera and the oscilloscope. A flag mounted on the falling weight interrupts the infrared radiation going from the LED to the photodiode, causing a trigger pulse. One switch is positioned so that it pulses when the tup hits the specimen. This triggers the oscilloscope and the pulsing of the laser used for the high speed camera. The camera's mechanical capping shutter must open before impact, thus a second switch is mounted higher on the tower to provide a trigger for the shutter 20 ms before impact.

The rotating mirror, high speed camera (see Figure 7) used for photographing the caustics can record 200 frames at up to 200,000 frames per second. In these experiments it was operated at a rate of 100,000 frames per second. Although it operates as a streak camera with no internal shuttering, discrete frames are obtained by pulsing the laser light source. Due to the short pulse width of the laser the exposure time of each frame is very

short (15 ns) resulting in sharp photographs. To photograph the caustics, the camera is placed in front of the specimen to collect the reflected light and is focused a distance z_0 behind the specimen. In order to use the J vs. D relation of Figure 5, the same z_0 value of 100 cm was used for these dynamic experiments as was used for the static experiments.

4.2 Results

Selected caustic photographs from the test of specimen 71 are shown in Figure 8. The time shown in the frames is the time in microseconds since impact. The values shown for J were obtained by measuring the caustic diameter,D, for each frame and then determining J from Figure 5.

The shape of the caustics obtained dynamically agrees very well with the shape of the caustics obtained statically, as can be seen through comparison of Figures 4 and 8. Only the last frame of Figure 8 which is elongated parallel to the crack does not correspond to the static results. As will be discussed later, this elongation is evidence of crack tunneling prior to fracture. The value of J corresponding to crack tunneling will be denoted here by J_t. Gross fracture initiation is defined here to have occurred when the crack has grown across the entire thickness of the specimen. The value of J corresponding to gross fracture initiation will be denoted here by J_i. Crack growth following tunneling in these thin, ductile specimens occurs in a shearing manner, i.e., the fracture surface is inclined at approximately 45° to the specimen surfaces as shown in Figure 9. The figure also shows that shear fracture is preceeded by an area of flat crack growth due to tunneling. This type of fracture surface was observed to produce an asymmetry in the caustic, causing the caustic to not close back on itself, similar to mixed mode caustics in linear elastic fracture. It is the appearance of this asymmetry that allows us to estimate the gross fracture initiation time and the corresponding value of J for gross fracture initiation.

The records of the time history of the J integral as measured with caustics are shown in Figure 10 for five tests, four at 5 m/s impact and one at 10 m/s impact. The results are given only up to the time of gross fracture initiation. It is seen that in comparison to the tup and support loads, shown in Figure 11, $J^d(t)$ increases in a smooth manner. The inertial effects tend to shield the crack tip from the highly dynamic impact loads. Similar results were reported by Kalthoff et al.[11] for experiments on linear elastic specimens. The

average loading rate of the 10 m/s impact specimen ($\dot{J} \approx 17 \times 10^8 N/m \cdot s$) is substantially higher than that of the 5 m/sec specimen ($\dot{J} \approx 6 \times 10^8 N/m \cdot s$). Even so, $J^d(t)$ is still relatively smooth. Good repeatability is demonstrated for $J^d(t)$ except during the time period from $320\mu s$ to $450\mu s$, where there is a discrepancy of 20% in J^d.

Accurate predictions of dynamic fracture initiation require data on dynamic fracture toughness obtained through experiments on initially notched and prefatigued specimens. Although no static experiments on fatigue cracked specimens were performed, so we cannot say precisely what the static fracture toughness of this material is, it is interesting to compare the fracture initiation values of J from the static and dynamic experiments.

Although the caustics clearly indicate the onset of unstable crack growth, there are some problems in exactly defining the fracture initiation time. There is evidence from strain gages fixed to the specimen near the crack tip and from the elongation of the caustics, see Fig. 8, that crack tunneling, or propagation of the crack in the interior of the specimen, occurs before gross crack initiation is observable on the specimen surface. By a careful analysis of the degree of elongation of the caustics, the time and the value of J, (J_t), where tunneling appears to begin was estimated. These values are summarized in Table 1. For the 5 m/s impact speeds $J_t \approx 240\, kN/m$, and for the 10 m/sec impact speeds $J_t \approx 380\, kN/m$. Tunneling was observed in the static experiments [25] at $J_t \approx 200 - 250\, kN/m$. The time that tunneling began was approximately $400\mu s$ for the 5 m/sec experiments. Note that it is in this very same time range that the $J^d(t)$ records disagree the most. If the initiation of tunneling occurs at slightly different times in each experiment, it may explain the discrepancies in $J^d(t)$. Crack tunneling changes the specimen stiffness resulting in different measured values of J^d.

Recent three-dimensional calculations by Narasimhan and Rosakis [27] show that the magnitude of stresses and strains near the crack tip, in the interior of the plastically deforming specimen are substantially higher than those near the surface. Such a distribution of deformation and stresses will clearly promote crack tunneling (see Figure 9). Further, experimental evidence demonstrating tunneling was obtained by first heat tinting and then breaking open at liquid nitrogen temperature (77°K) a specimen that was previously loaded statically at room temperature to just below the gross fracture initiation load. The

crack was found to have tunneled 6 mm in the center of the specimen.

It is interesting to note that some preliminary three-dimensional calculations by Narasimhan, Rosakis and Moran [29] based on a damage accumulation model of the Gurson type, predict that crack tunneling will initiate when $\hat{J}$ at the center plane of the specimen is equal to $250\,kN/m$. Using the through the thickness distribution of $\hat{J}$ in [27], this value of $\hat{J}$ corresponds to an average value of J of $210\,kN/m$; remarkably close to the experimental values of $J = 240kN/m$.

In the static experiments [25] on specimens with EDM cut crack tips, it was found that $J_i \approx 420\,kN/m$. In the present experiments when the impact speed was 5 m/s, $J_i \approx 350\,kN/m$ regardless of the crack tip condition. For the higher rate of loading, the toughness appears to be greater, $J_i \approx 420\,kN/m$. Unfortunately, from this limited data, no trends can be drawn regarding gross fracture toughness as a function of loading rate.

The results of these experiments indicate that it is possible to measure the J integral dynamically using the method of caustics regardless of the loading rate. Nonetheless one must ask whether the accuracy of this technique will be affected by inertial effects and by material strain rate sensitivity. From the dynamic finite element analysis to be discussed in section 6, the strain rates at a distance of about 2 mm from the crack tip were estimated to be of the order of $10^1 s^{-1}$ for the 5 specimens corresponding to 5 m/s impact speed. High strain rate experiments on a similar heat treatment of 4340 steel [24] show that the rate sensitivity of this material is relatively low and would result in an increase in flow stress of less than 7% for strain rates of the same order as above. Thus rate sensitivity will not affect the accuracy of the present experiments, although it may affect similar experiments involving highly rate sensitive metals.

In the next section the accuracy of the results obtained by caustics will be examined further, through comparisons with analytical and dynamic numerical models simulating the experiments.

5. COMPARISON WITH THE MASS-SPRING MODEL

A back of the envelope type of calculation of $J^d(t)$ can be achieved by using a lumped mass-spring model of the experiments. This calculation provides only an approximate verification of the caustics results for $J^d(t)$.

Williams [30,31] recently suggested that dynamic fracture problems may be adequately analyzed by means of lumped mass-spring models. For this analysis Williams' system was modified by using a single spring, single mass model as sketched in Fig. 12. The stiffness K of the model is chosen to be the stiffness of the actual test specimen ($5 \times 10^7 N/m$). The effective mass, m, of the model is chosen so that the kinetic energy, T, of the model and of the specimen will be identical when the model and the specimen have equal load point displacement rates, $\dot{\delta}(t)$; see [30] for details. Following [30], the effective mass, m, is found to be $17/35 \cdot M$, where M is the actual mass of the specimen ($m = 0.88kg$).

The load $P(t)$ applied to the mass is the measured tup load for the experiment, Fig. 11. The displacement $\delta(t)$ is calculated from the mass-spring model. The reaction force $P_1(t)$ of the spring is then given by $P_1(t) = K\delta(t)$. The J integral is estimated by treating the model as if it was a linear elastic specimen subjected to quasi-static loading, i.e.,

$$J^d(t) = \frac{P_1^2(t)}{E} \cdot f,$$

where f is a function of specimen geometry, given in [32], that relates J to the applied loads for static problems, and E is the elastic modulus.

Using the above procedure the tests for specimen 71 (5 m/s impact) and for specimen 75 (10 m/s impact) were analyzed. The results, shown here in Fig. 13, compare the caustics results to the mass-spring model. It is seen that on the average the mass-spring model agrees well with the caustics results for both loading rates. The agreement is poorest at shorter times ($t < 400\mu s$), when strong stress wave effects dominate. In this time range the simple mass-spring model is not expected to capture the complete dynamic behavior of the specimen. On the other hand, for $t > 400\mu s$, the model and the experimental results agree well despite the simplistic linear nature of the mass-spring model. Nevertheless, despite this agreement, final verification of the proposed optical procedure must be obtained through dynamic, elastic-plastic, finite element simulation of the experiment.

6. DYNAMIC FINITE ELEMENT ANALYSIS

To provide a more reliable verification of the experimental results, an elastic-plastic, two-dimensional dynamic finite element simulation was performed.

The experimentally measured tup and support loads, given in Fig. 11 for specimen 71, were used as the traction boundary conditions for the simulation. One half of the specimen was modeled using a J_2 incremental plasticity theory with isotropic hardening and a piecewise power hardening law, which for loading in uniaxial tension takes the form of equation (3.1). The values of σ_0 and n are 1030 MPa and 22.5, corresponding to the particular heat treatment of 4340 used here (see section 4). The dynamic J integral was computed using the domain integral formulation of Shih et al. [7].

The resulting $J^d(t)$ record from the finite element analysis is shown in Fig. 14 along with the caustics results up to 400 μs. The time of 400 μs corresponds with the time that crack tunneling begins as detected by the elongation in the caustic shapes. Since the two-dimensional finite element analysis cannot model tunneling, it will clearly be inapplicable for longer times. The analysis and the experimental results agree very well in this time range. It might be of interest to note here that at the time when the experimental results indicated tunneling, the numerical calculation, if carried further, deviates from the experimental measurements. Also note that there is a great deal of high frequency oscillation in the finite element results. This is a consequence of the high frequency noise in the tup and support load records, Fig. 11, that were used as traction boundary conditions. Much of the high frequency noise represents the dynamic response of the tup and supports and thus does not represent the true boundary loads.

The conclusions that we draw from the good agreement of the experimental and numerical results for $J^d(t)$ is that interpretation of the dynamic caustics in terms of the static calibration procedure provides an accurate measure of $J^d(t)$ up to the time when crack tunneling begins. After crack tunneling begins the numerical analysis provides no confirmation of the caustics results, and in addition J loses its strict meaning as a fracture parameter.

7. PROCEDURE FOR THE MEASUREMENT OF J^d.

The favorable agreement between $J^d(t)$ measured by caustics and calculated by the dynamic finite element model (section 6) leads us to propose a procedure for the dynamic measurement of J in arbitrary dynamic loading. This procedure is outlined as follows:

1. To determine the dynamic fracture toughness of a given material, select a planar test specimen geometry that is amenable to both static and dynamic loading.
2. Perform a static experiment to determine the relationship between the J integral and the caustic diameter, D, for loads up to fracture initiation and for a fixed value of z_0. The J integral may be determined through standard load-displacement methods as discussed in section 3. A three dimensional elastic-plastic finite element analysis is not necessary for this step, although one was performed for the current investigation.
3. Use the same specimen geometry and material in a dynamic test, such as drop weight impact.
4. Use a high speed camera to record caustics for a duration at least as long as the fracture initiation time, using the same z_0 as was used for the static experiments.
5. Use the J vs. D calibration of step 2 to interpret the caustics and obtain the time history of $J^d(t)$. Examination of changes in caustic shape can be used to provide the time of crack initiation (see section 4).

ACKNOWLEDGMENTS

Support of the Office of Naval Research through contract N00014-85-K-0599 is gratefully acknowledged. The computations were performed using the facilities of the San Diego Supercomputer Center and are made possible through an NSF-DYI grant MSM-84-51204 to the second author. The authors would like to acknowledge the contribution of Mr. R. Pfaff toward the upgrading of the high speed camera. The second author would also like to acknowledge his many useful discussions with L. B. Freund.

References

[1] J. R. Rice, *Journal of Applied Mechanics*, 35 (1968) 379-386.

[2] J. W. Hutchinson, *Journal of the Mechanics and Physics of Solids*, 16, (1968) 13-31.

[3] J. R. Rice and G. F. Rosengren, *Journal of the Mechanics and Physics of Solids*, 16 (1968) 1-12.

[4] B. Budiansky and J. R. Rice, *Journal of Applied Mechanics*, 40 (1973) 201-203.

[5] B. Broberg, *Journal of Applied Mechanics*, 54 (1987)458-459.

[6] F. Li, C. F. Shih, and A. Needleman, *Engineering Fracture Mechanics*, 21 (1985) 405-421.

[7] C. F. Shih, B. Moran, and T. Nakamura, *International Journal of Fracture*, 30 (1986) 79-102.

[8] T. Nakamura, C. F. Shih, and L. B. Freund, *Engineering Fracture Mechanics*, 25 (1986) 323-339.

[9] L. S. Costin, J. Duffy, and L. B. Freund, in *Fast Fracture and Crack Arrest, ASTM STP 627*, American Society for Testing and Materials (1977) 301-318.

[10] T. Nakamura, C. F. Shih, and L. B. Freund, *Engineering Fracture Mechanics* 22 (1985) 437-452.

[11] J. F. Kalthoff, W. Bohme, S. Winkler, W. Klemm, in proceedings of CSNI Specialist Meeting on Instrumented Precracked Charpy Testing, Electric Power Research Institute, Palo Alto, CA (1980).

[12] A. T. Zehnder and A. J. Rosakis, "Dynamic Fracture Initiation and Propagation in 4340 Steel under Impact Loading", Caltech report SM86-6, submitted to *International Journal of Fracture* (1988).

[13] A. S. Douglas and M. S. Suh, "Impact fracture of a tough ductile steel", to appear in proceedings of the 21sr ASTM National Fracture Symposium, AnNapolis, Maryland, June 1988.

[14] W. N. Sharpe, Jr., A. S. Douglas and J. M. Shapiro, "Dynamic fracture toughness evaluation by measurement of C.T.O.D.", Johns Hopkins Mechanical Engineering Report WNS-ASD-88-02, February 1988.

[15] P. Manogg, Ph. D. Thesis, Freiburg, West Germany (1964).

[16] P. S. Theocaris, in *Mechanics of Fracture, Vol. VII*, G. Sih (ed.), Sijthoff and Noordhoff (1981) 189-252.

[17] A. J. Rosakis and L. B. Freund, *Journal of Engineering Materials and Technology* 104 (1982) 115-120.

[18] A. J. Rosakis, C. C. Ma, and L. B. Freund, *Journal of Applied Mechanics* 50 (1983) 777-782.

[19] A. T. Zehnder, A. J. Rosakis, and R. Narasimhan, to appear in *Nonlinear Fracture Mechanics, ASTM STP 995*, American Society for Testing and Materials (1988).

[20] A. T. Zehnder, Ph. D. Thesis, California Institute of Technology (1987).

[21] A. J. Rosakis and A. T. Zehnder, *Journal of Elasticity* 15 (1985) 347-367.

[22] M. L. Willliams, *Journal of Applied Mechanics*, 24 (1957) 109-114.

[23] J. Beinert and J. F. Kalthoff, in *Mechanica of Fracture, Vol. VII*, G. Sih (ed.), Sifthoff and Noordhoff (1981) 281-320.

[24] S. Tanimura and J. Duffy, *International Journal of Plasticity*, 2 (1986) 21-35.

[25] A. T. Zehnder and A. J. Rosakis, "Three Dimensional Effects near a Crack Tip in a Ductile Three-Point Bend Specimen Part II: An Experimental Investigation Using Interferometry and Caustics", Caltech report SM88-7, submitted to *Journal of Applied Mechanics* (1988).

[26] J. R. Rice, P. C. Paris and J. G. Merkle, in *Progress in Flaw Growth and Fracture Toughness Testing, ASTM STP 536*, American Society for Testing and Materials (1973) 231-245.

[27] R. Narasimhan and A. J. Rosakis, "Three Dimensional Effects near a Crack Tip in a Ductile Three Point Bend Specimen Part I: A Numerical Investigation", Caltech report SM88-6, submitted to *Journal of Applied Mechanics* (1988).

[28] R. Narasimhan and A. J. Rosakis, *Journal of the Mechanics and Physics of Solids* 36 (9188) 77-117.

[29] R. Narasimhan, A. J. Rosakis, and B. Moran, Caltech Report (1989).

[30] J. G. Williams, *International Journal of Fracture* 33 (1987) 47-59.

[31] J. G. Williams and G. C. Adams, *International Journal of Fracture* 33 (1987) 209-222.

[32] H. Tada, P. C. Paris, and G. Irwin, *The Handbook of Stress Intensity Factors*, Del

Research Corporation (1973).

Table I, Summary of Experiments

Specimen	Crack Tip	Impact Speed	Tunneling		Gross initiation	
		m/S	J_t,kN/m	t,μs	J_i,kN/m	t,μs
70	0.3 mm dia.	5	240	400-500	350	650-700
71	0.3 mm dia.	5	240	400-500	350	650-700
74	fatigue	5	250	400-500	350	650-730
75	fatigue	10	380	320-370	500	370-430
77	0.3 mm dia.	5	250	400-510	420	680-800

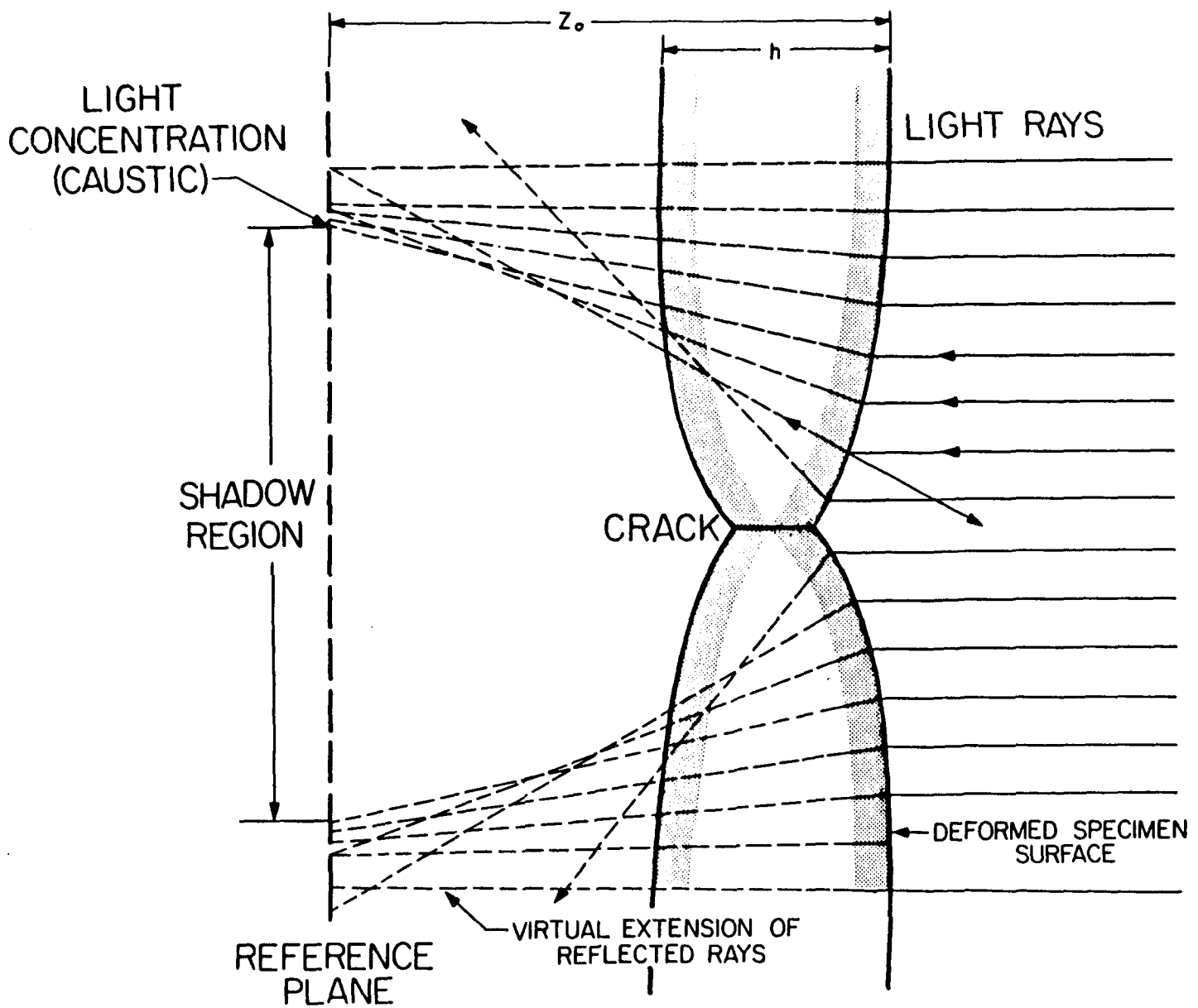

Fig. 1 Formation of caustic due to reflection of light from the polished deformed specimen surface near a crack tip.

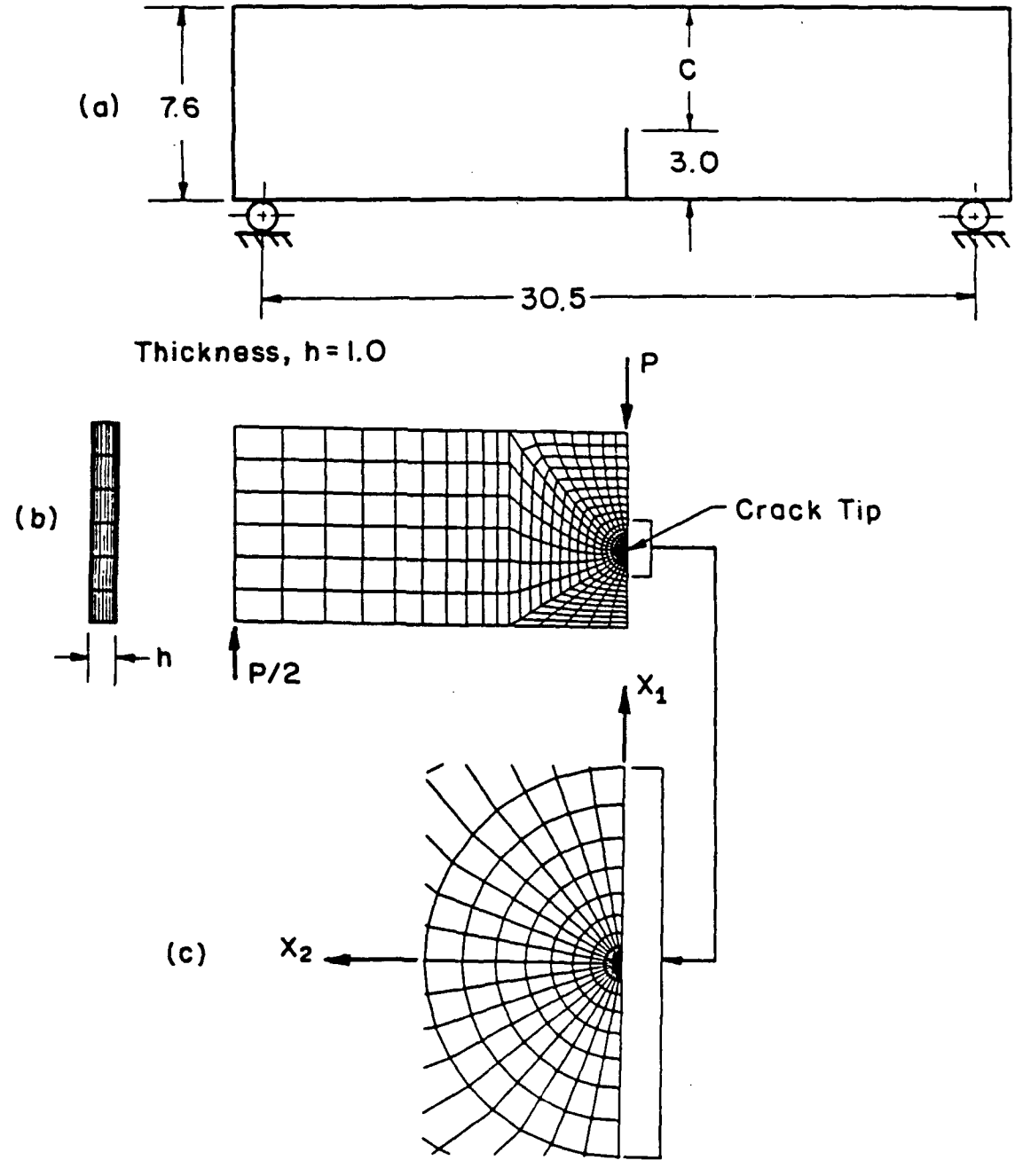

Fig. 2 Three point bend test specimen. All dimensions are in cm.

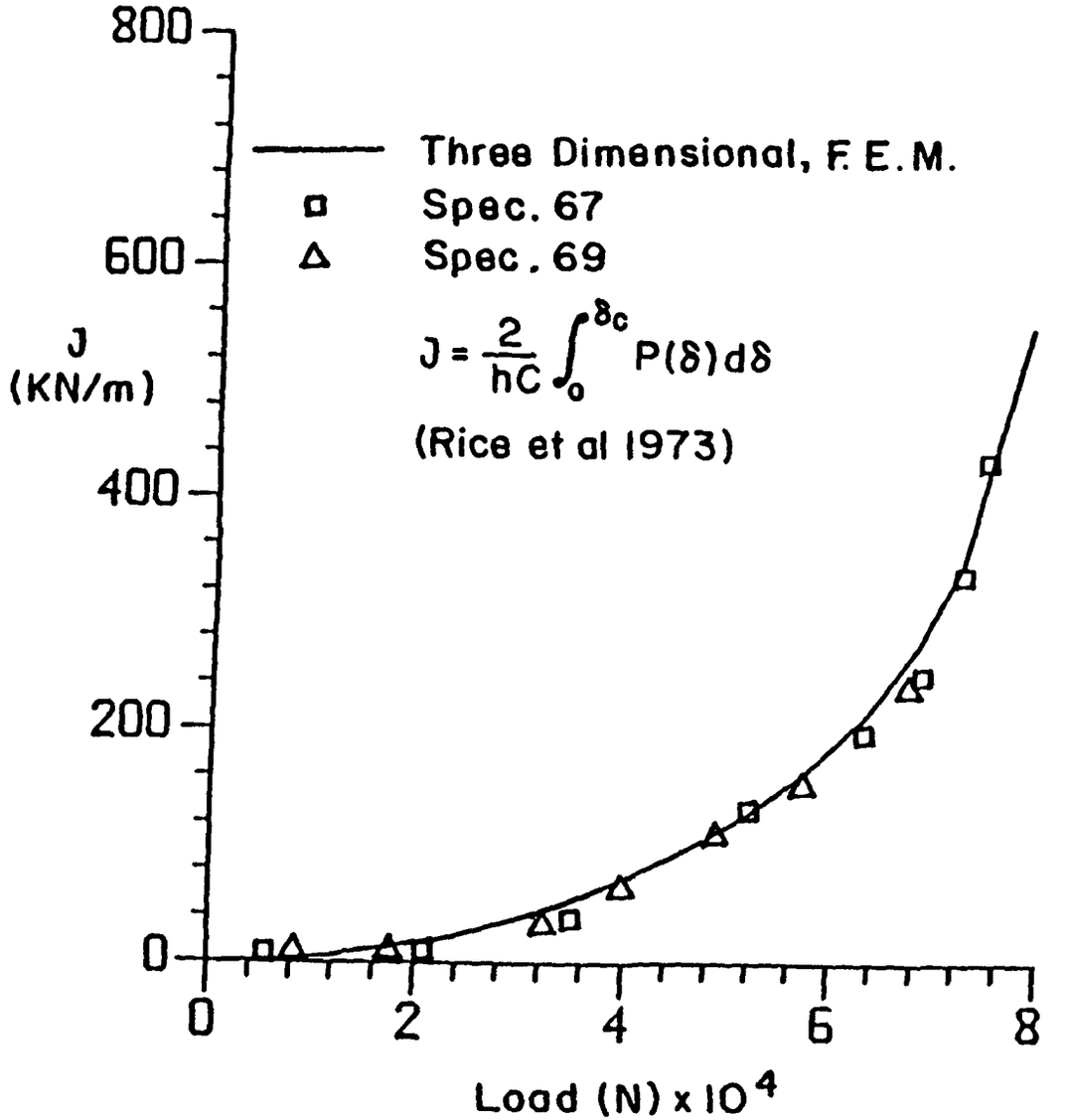

Fig. 3 J integral versus applied load for static experiments. J calculated numerically and from experimental load-load point displacements.

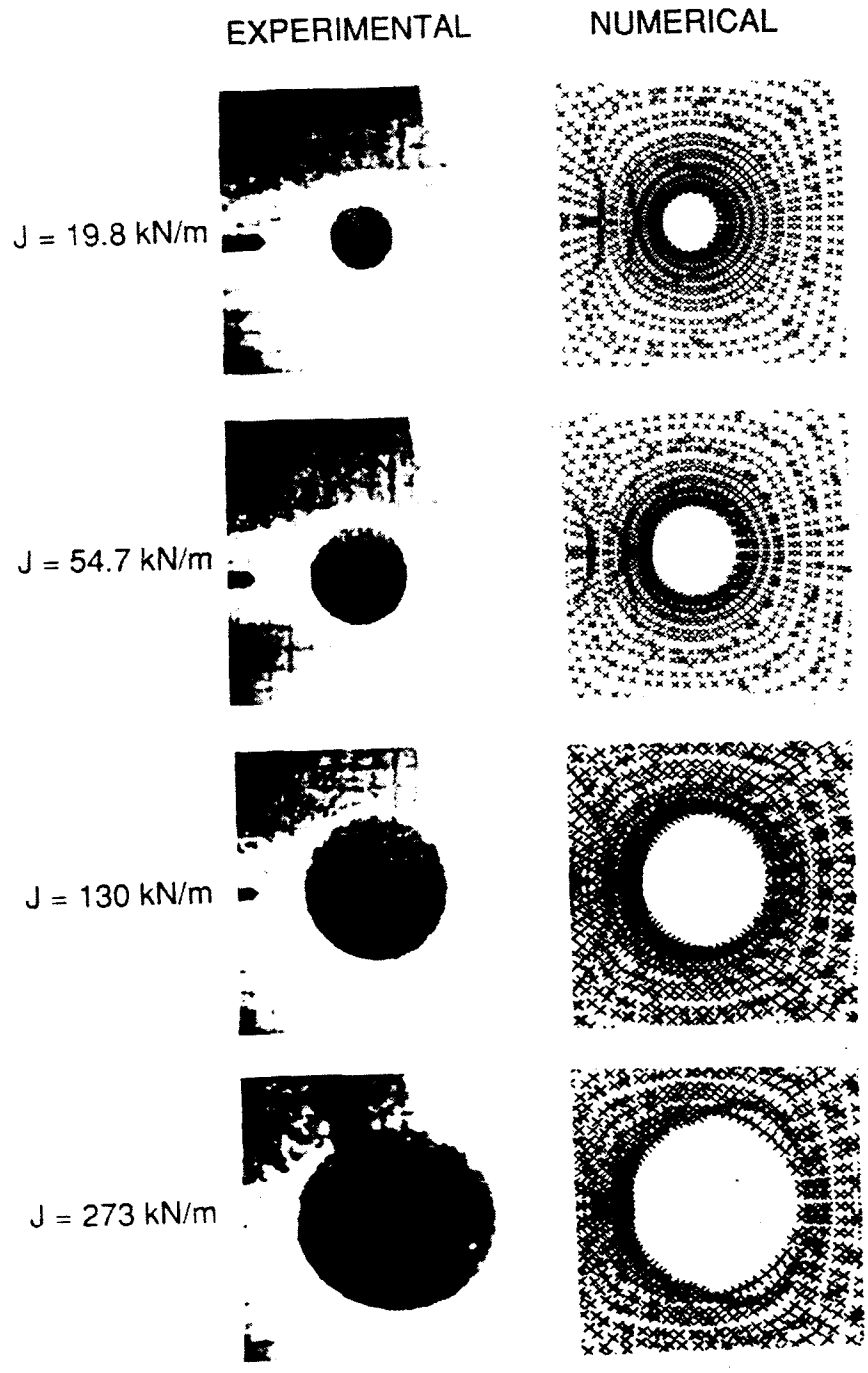

Fig. 4 Sequence of caustics for static experiment, $z_0 = 100cm$. Experimental results and results from 3-D numerical analysis.

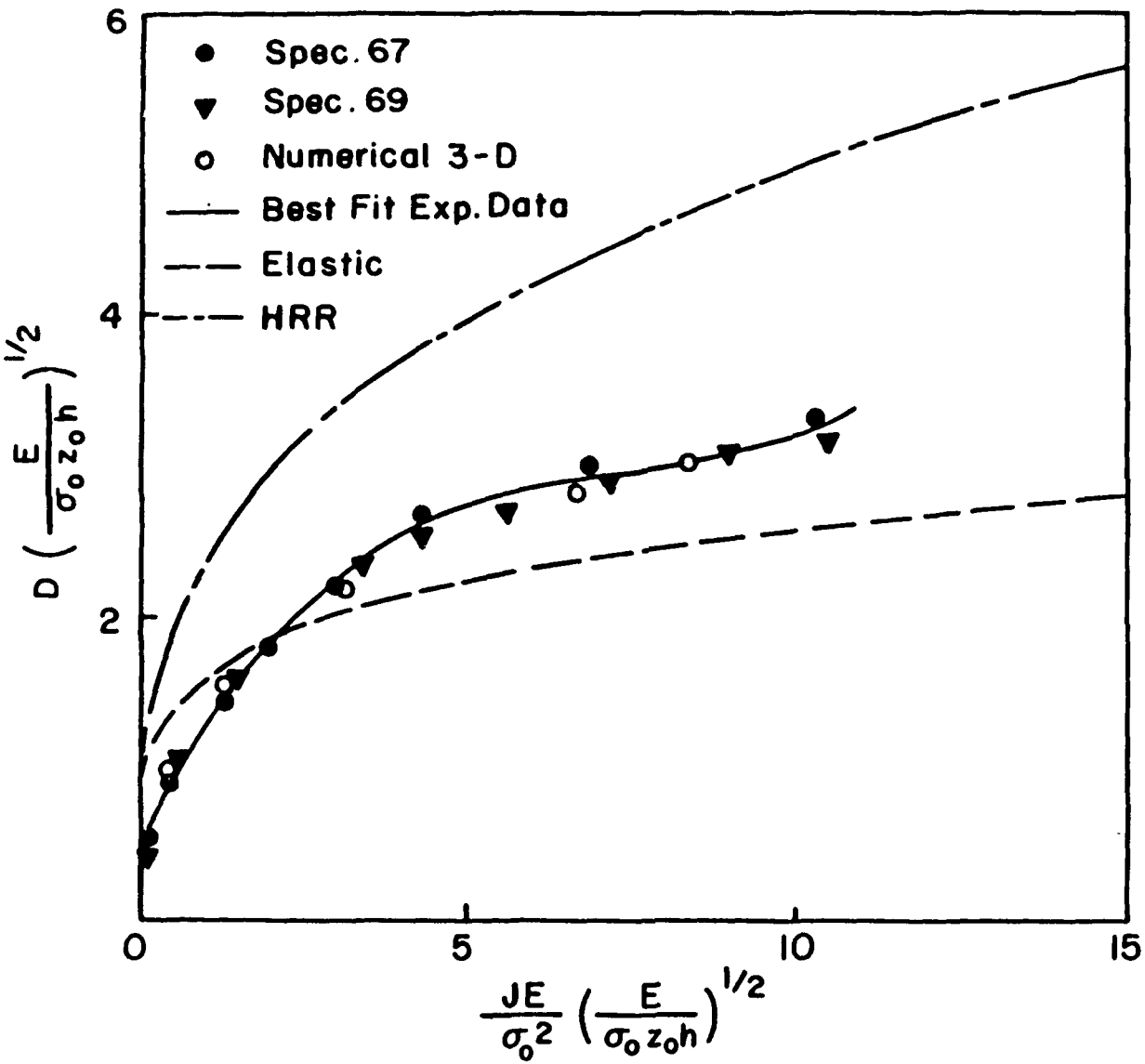

Fig. 5 Relation between caustic diameter, D, and J integral. Experimental and 3-D numerical results are shown.

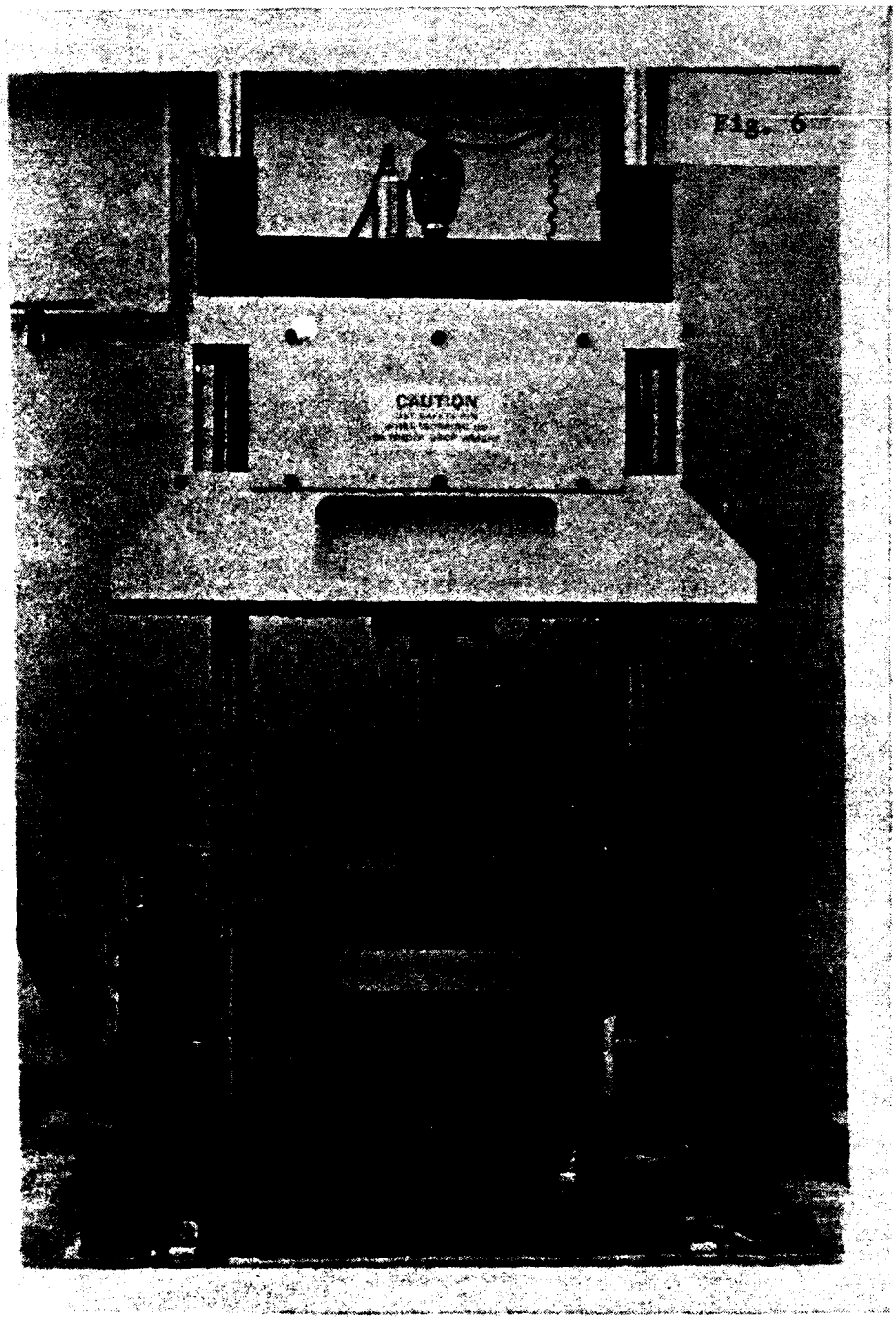

Fig. 6 Photograph of specimen and drop weight tower.

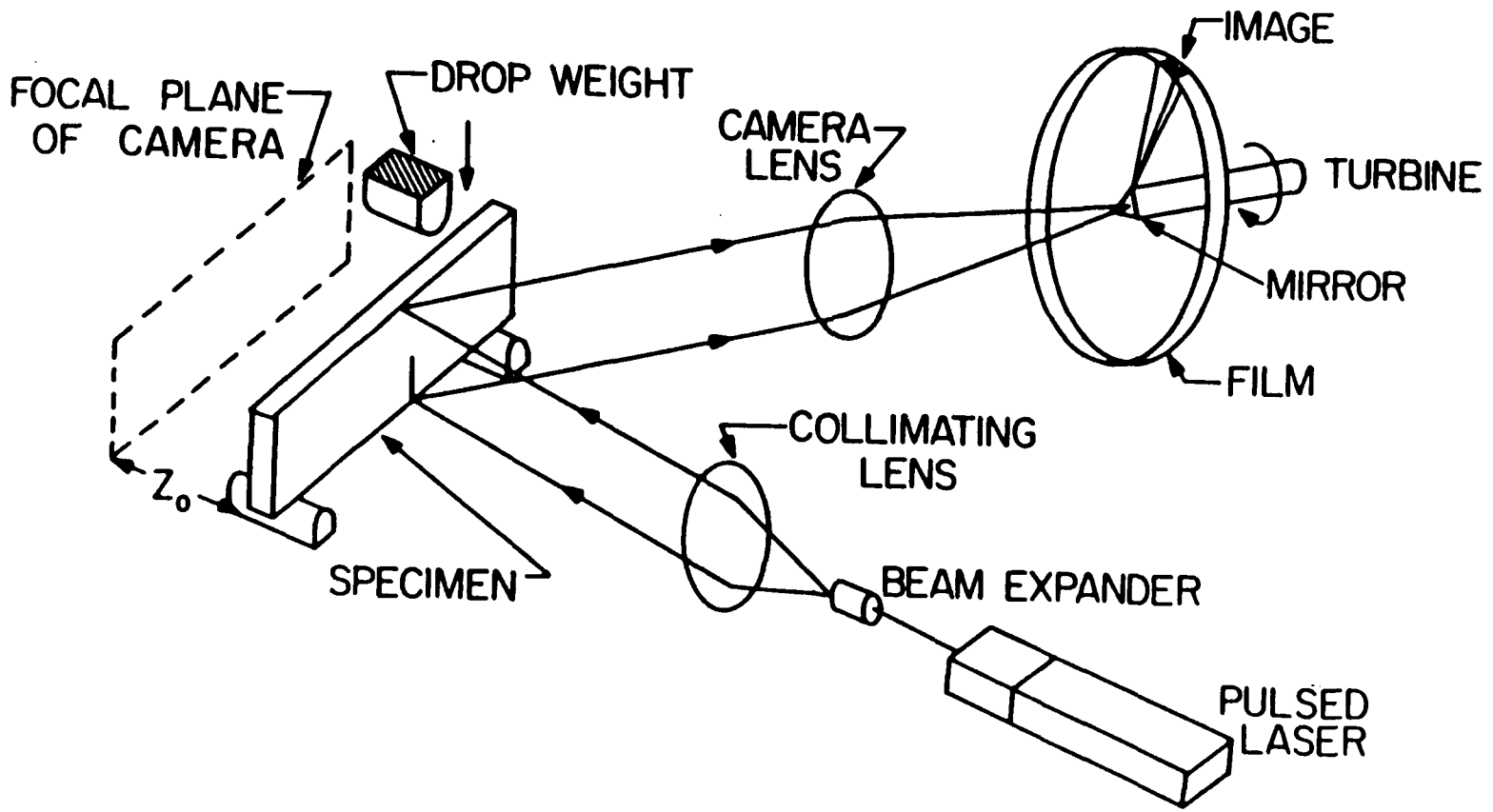

Fig. 7 Setup for fracture initiation experiments using drop weight loading and using high speed photography to record caustics formed by reflection.

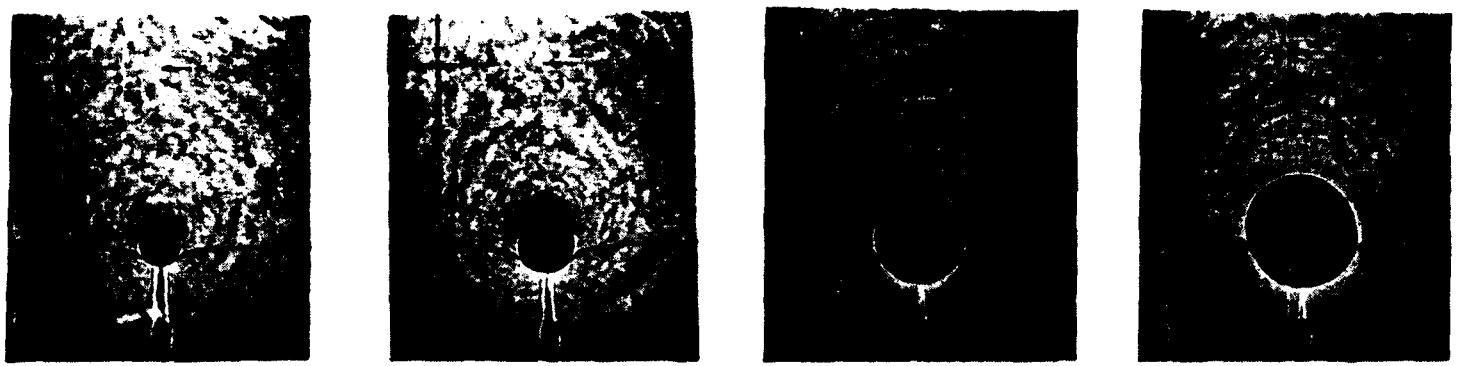

37 μs
$J = 5\ kN/m$

57 μs
$J = 11\ kN/m$

107 μs
$J = 38\ kN/m$

247 μs
$J = 70\ kN/m$

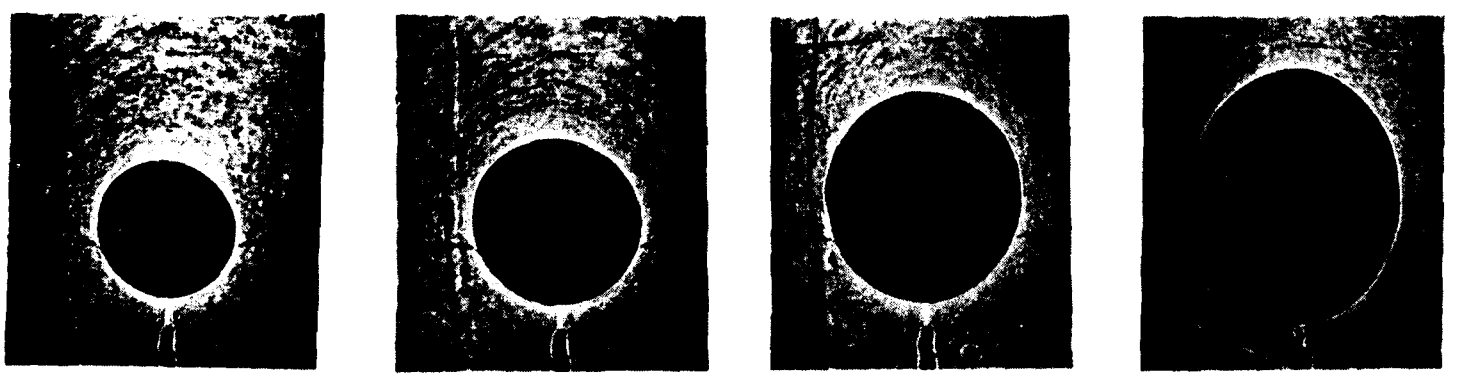

277 μs
$J = 120\ kN/m$

317 μs
$J = 196\ kN/m$

497 μs
$J = 284\ kN/m$

687 μs
$J = 345\ kN/m$

Fig. 8 Sequence of caustics photographed during dynamic experiment, specimen 71.

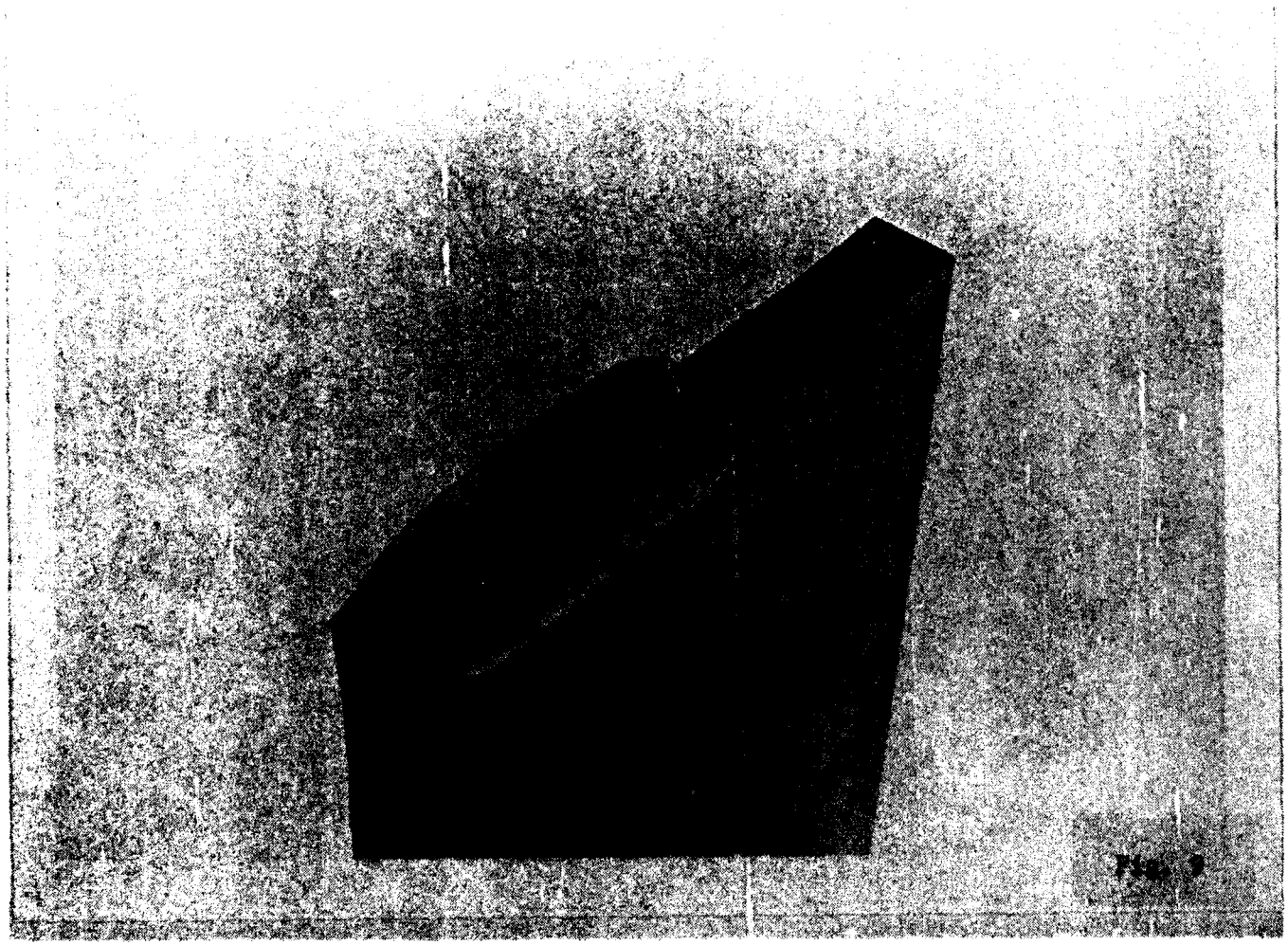

Fig. 9 Photograph of fracture surface of 4340 steel specimen broken under impact loading.

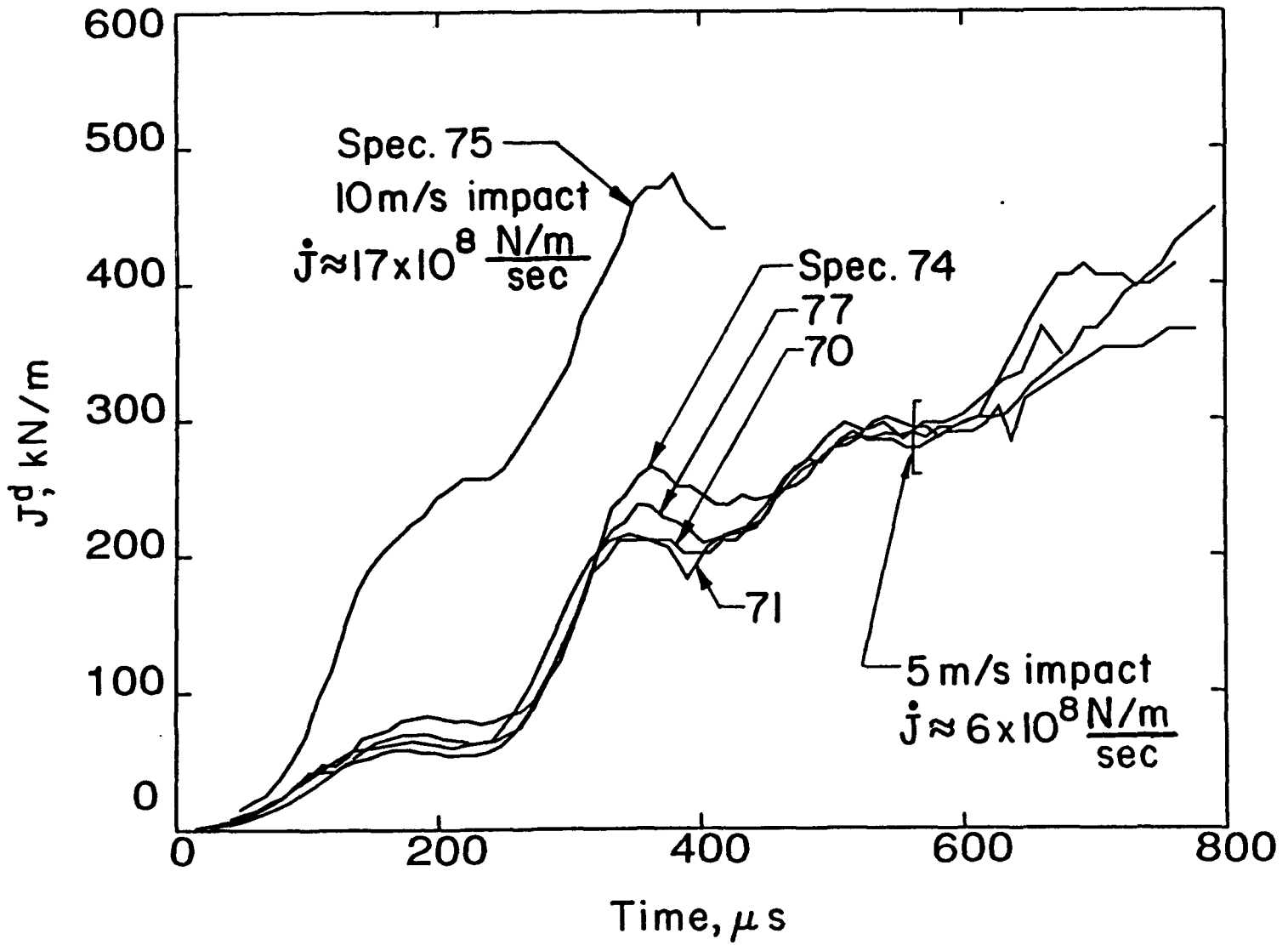

Fig. 10 $J^d(t)$ record from caustics for two loading rates. Data given up to time of fracture initiation.

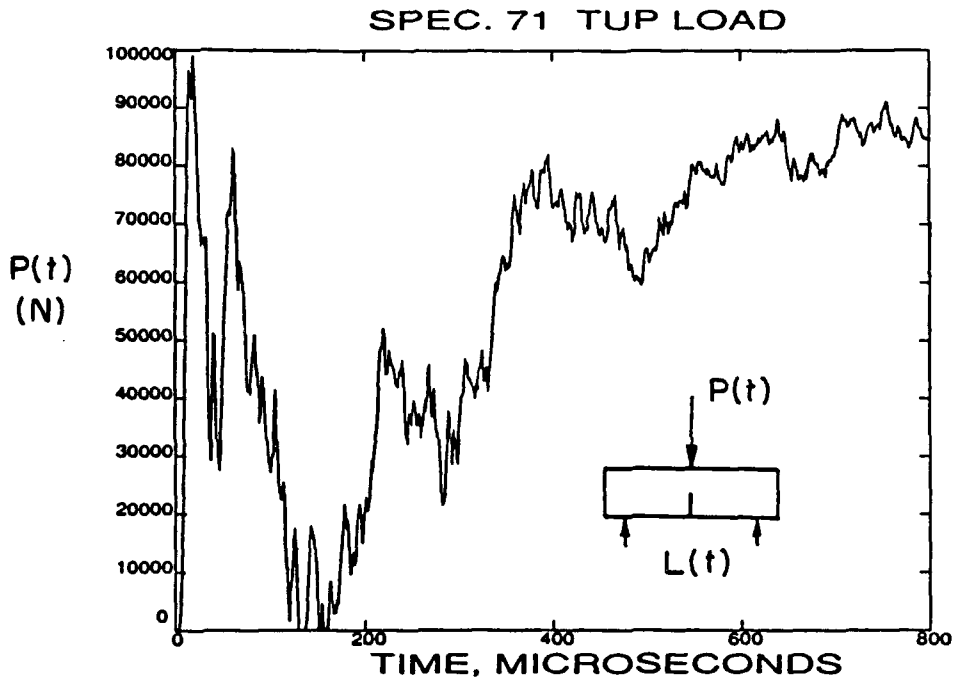

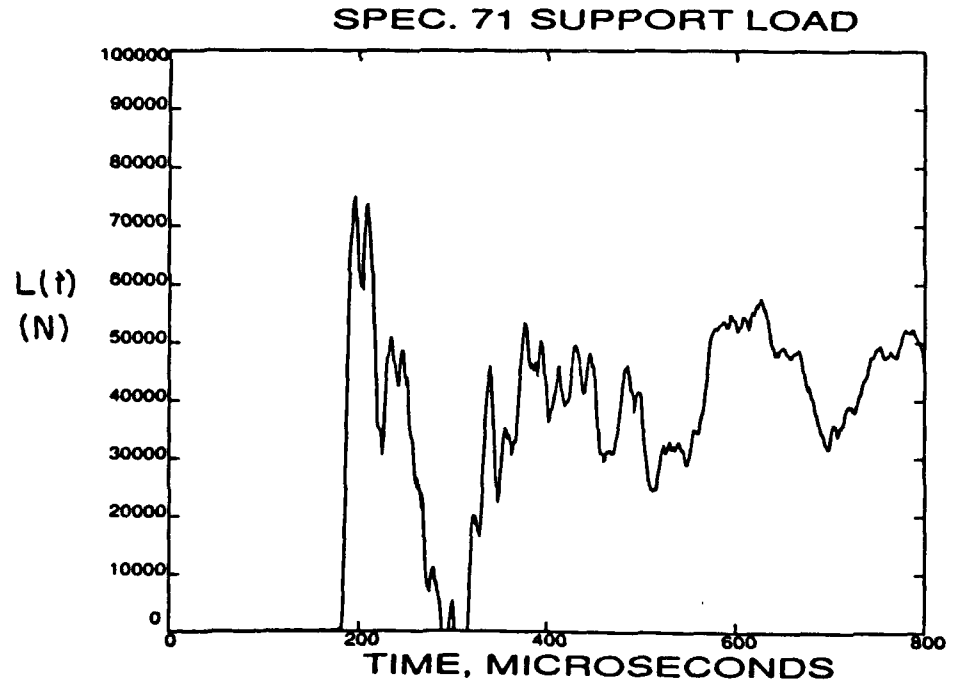

Fig. 11 Load records for specimen 71. (a) Tup load. (b) Support load.

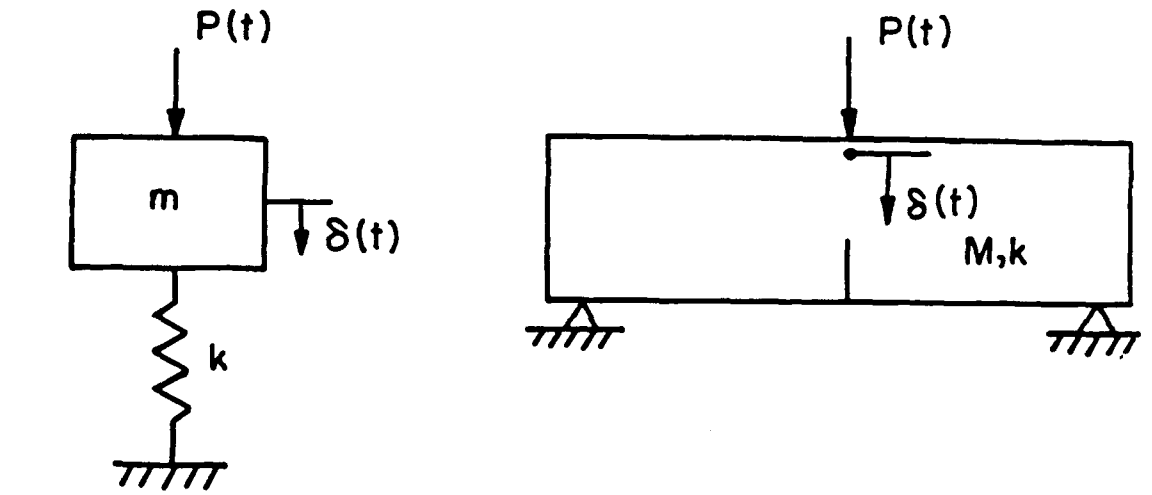

Fig. 12 Lumped mass-spring model of drop weight tests.

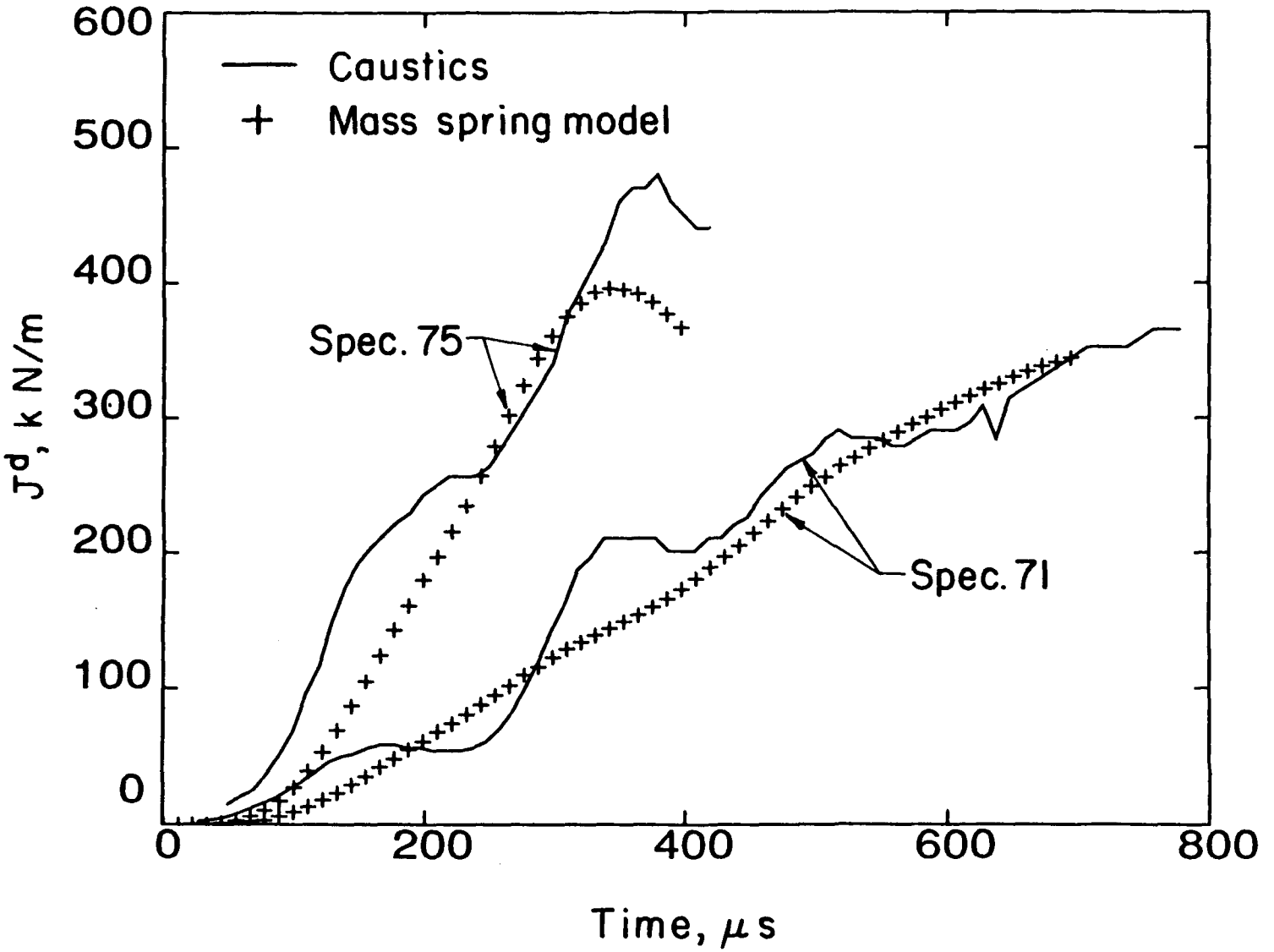

Fig. 13 Comparison of $J^d(t)$ from mass-spring model and from caustics for two loading rates.

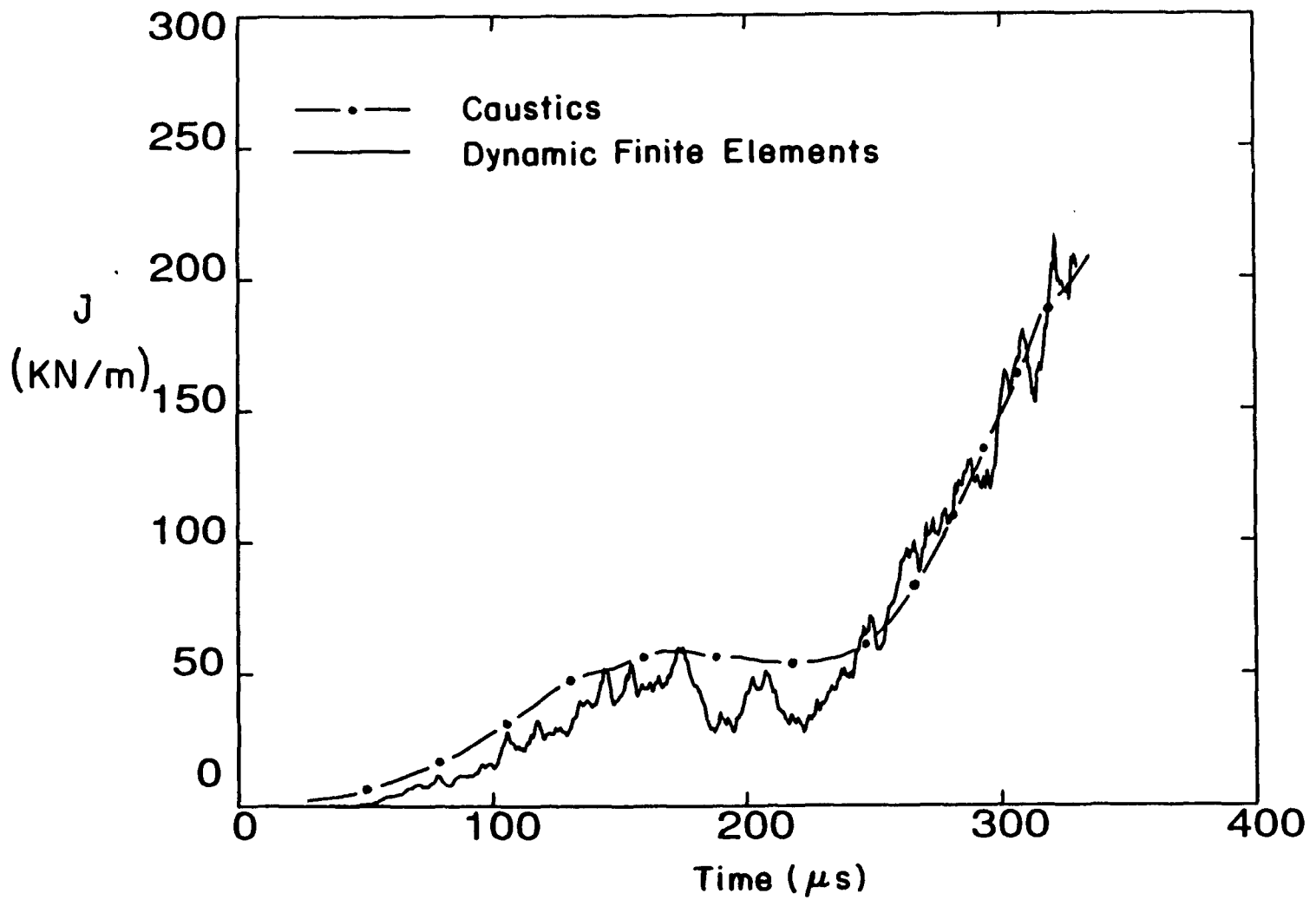

Fig. 14 Comparison of $J^d(t)$ from 2-D, dynamic, elastic-plastic finite element calculation and from caustics.

SECURITY CLASSIFICATION OF THIS PAGE (When Data Entered)

REPORT DOCUMENTATION PAGE

READ INSTRUCTIONS BEFORE COMPLETING FORM

1. REPORT NUMBER: SM 88-8

2. GOVT ACCESSION NO.:

3. RECIPIENT'S CATALOG NUMBER:

4. TITLE (and Subtitle): Dynamic Measurement of the J Integral in Ductile Metals: Comparison of Experimental and Numerical Techniques

5. TYPE OF REPORT & PERIOD COVERED:

6. PERFORMING ORG. REPORT NUMBER:

7. AUTHOR(s): Alan T. Zehnder, Ares J. Rosakis and Sridhar Krishnaswamy

8. CONTRACT OR GRANT NUMBER(s): ONR Contract N00014-85-J-0596

9. PERFORMING ORGANIZATION NAME AND ADDRESS: Graduate Aeronautical Laboratories, 105-50 California Institute of Technology Pasadena, CA 91125

10. PROGRAM ELEMENT, PROJECT, TASK AREA & WORK UNIT NUMBERS:

11. CONTROLLING OFFICE NAME AND ADDRESS: Dr. Yapa Rajapakse, Program Manager ONR, Code 1132SM, 800 N.Quincy St.,Arlington,VA 22217-5000

12. REPORT DATE: August 1988

13. NUMBER OF PAGES: 40

14. MONITORING AGENCY NAME & ADDRESS(if different from Controlling Office):

15. SECURITY CLASS. (of this report): Unclassified

15a. DECLASSIFICATION/DOWNGRADING SCHEDULE:

16. DISTRIBUTION STATEMENT (of this Report):

17. DISTRIBUTION STATEMENT (of the abstract entered in Block 20, if different from Report):

18. SUPPLEMENTARY NOTES: To appear in the International Journal of Fracture

19. KEY WORDS (Continue on reverse side if necessary and identify by block number): Dynamic fracture, elastic-plastic fracture, the method of caustics, finite-element analysis.

20. ABSTRACT (Continue on reverse side if necessary and identify by block number):

Experiments and analyses designed to develop an extension of the method of caustics to applications in dynamic, elastic-plastic fracture mechanics are described. A relation between the caustic diameter, D, and the value of the J Integral was obtained experimentally and numerically for a particular statically loaded specimen geometry (three point bend) and material (4340 steel). Specimens of the same geometry and material were then loaded dynamically in impact. The resulting caustics, recorded using high speed photography were analyzed on the basis of the J versus D relation to determine the

DD FORM 1 JAN 73 1473 EDITION OF 1 NOV 65 IS OBSOLETE

S/N 0102-LF-014-6601

SECURITY CLASSIFICATION OF THIS PAGE (When Data Entered)

time history of the dynamic value of J, $J^d(t)$. The history of J^d thus obtained is compared with good agreement to an independent determination of $J^d(t)$ based on two dimensional, dynamic, elastic-plastic finite element analysis, which used the experimentally measured loads as traction boundary conditions.